Calcium carbonate casein-based composite microspheres with mycogenic copper nanoparticles: synthesis, characterization and plant growth promotion

Nanotechnology

OPEN ACCESS

RECEIVED
15 June 2026

REVISED
28 July 2026

ACCEPTED FOR PUBLICATION
14 August 2026

PUBLISHED
9 September 2026

PAPER

Calcium carbonate casein-based composite microspheres with mycogenic copper nanoparticles: synthesis, characterization and plant growth promotion

Julia Nadrowska[1,2], Joanna Trzcińska-Wencel[1,2], Patrycja Golińska[1,2], Marek Wiśniewski[2,3], Sudhir Shende[1,2] and Aniket Gade[1,2,4,*]

[1] Department of Microbiology, Faculty of Biological and Veterinary Sciences, Nicolaus Copernicus University in Toruń, Lwowska 1, 87-100 Toruń, Poland
[2] Institute of Advanced Studies, Nicolaus Copernicus University in Toruń, Wileńska 4, 87-100 Toruń, Poland
[3] Department of Chemistry of Materials, Adsorption and Catalysis, Faculty of Chemistry, Nicolaus Copernicus University in Toruń, Gagarina 7, 87-100 Toruń, Poland
[4] Present address: Department of Biological Sciences and Biotechnology, Institute of Chemical Technology, Mumbai, Maharashtra 400019, India.
[*] Author to whom any correspondence should be addressed.

E-mail: aniket.gade@umk.pl

Keywords: biogenic nanoparticles, plant growth stimulation, crop protection, calcium carbonate microsphere, casein micelle, nanofertilizer

Supplementary material for this article is available online

Abstract

Nanotechnology offers a promising approach by enabling slower, controlled release of fertilizer, improving nutrient uptake, and reducing the overall quantity of fertilizer needed, compared to conventional chemical fertilizers, which are often inefficient, require intensive application, and often lead to nutrient leaching into the soil. Copper nanoparticles (CuNPs) were synthesized using *Fusarium graminearum* autolysate, then complexed with casein micelles (CuMC), and subsequently CuMC were encapsulated within calcium carbonate composite microspheres (CuMS). Maize was treated with Hoagland solution containing a copper source substituted with CuNPs, CuMC, or CuMS. After 30 d, the plantlets were harvested, their length and fresh and dry weight were measured, and copper content and leaf chlorophyll content were assessed. CuNPs were spherical, small, negatively charged, showing a cubic phase structure, with biomolecules on their surface, and exhibited promising antimicrobial activity. CuMC were spherical with an average diameter of 133.65 nm, while CuMS were mesoporous with a mean size of 1.09 μm. The treatment of maize with CuMC increased the fresh weight of stems and roots by 15%–20%, while CuMS increased the fresh weight of leaves, stems, and roots, as well as the dry weight of leaves by 14%–32%. Application of CuNPs, CuMC, and CuMS resulted in higher chlorophyll content (9%–24%), whereas CuNPs treatment increased copper concentration (15%–42%). CuMC and calcium carbonate CuMS serve as effective carrier materials that encapsulate CuNPs and slow their degradation rate. CuNPs-based composites enhance maize growth and increase chlorophyll content, demonstrating great potential as environmentally friendly nanofertilizers for agricultural applications.

1. Introduction

One of the challenges in modern agriculture is the limited availability of nutrients for plants, which negatively impacts crop yield and the nutritional quality of agricultural products, ultimately contributing to malnutrition in humans and animals [1]. However, chemical fertilizers used to supplement micro- and macroelements exhibit low uptake efficiency and thus must be applied in large amounts, with a substantial portion leaching into soil and water ecosystems [2]. Copper plays an essential role in plants, as it is

vital for various physiological processes, including photosynthesis, cellular respiration, cell wall synthesis, and protection against oxidative stress [3]. Deficiency of this micronutrient leads to reduced productivity and inferior crop quality, often manifested as smaller fruits, leaf chlorosis, or diminished flavor [4]. Although copper is indispensable for optimal plant growth and development, in excessive concentrations it can stunt plant growth and disrupt cellular processes. Its dual nature—as both an essential and potentially toxic element—underscores the importance of precise control of fertilizer dosage [5]. Nanotechnological solutions can be employed to achieve slower, controlled fertilizer release, thereby enhancing nutrient uptake while minimizing the amount of product used [2, 6].

Nanoparticles, defined as particles with all three dimensions smaller than 100 nm, possess a high surface area-to-volume ratio that imparts unique structural, optical, and electronic properties compared to materials in the micro- and macroscale [7–9]. Mycosynthesis is environmentally friendly, safer, and simpler than physical and chemical methods, as it does not require hazardous conditions such as high temperature, high pressure, or toxic chemicals [10]. Fungi are particularly suitable for metal nanoparticle synthesis due to their high metal tolerance, ability to accumulate metals, and secretion of diverse metabolites—such as enzymes and proteins—that act as reducing and stabilizing agents. Additional advantages include rapid growth, abundant biomass production, and simple biomass processing, making fungal-mediated synthesis both economically viable and scalable [11–13].

Due to their unique properties, biogenic nanoparticles have strong potential for agricultural applications. However, encapsulation, as the process of enclosing or coating a core material with another substance to form a protective shell that safeguards active ingredients from external environmental factors, can improve the effectiveness of nanoparticles [14]. Interestingly, casein—a phosphorylated protein found in milk—offers several advantages as a carrier material. It is a non-toxic, biodegradable, easily accessible, and inexpensive natural polymer. Casein exhibits high thermostability, even above 100 °C, due to its lack of tertiary structure. It can also self-assemble into micelles in the presence of calcium phosphate [15, 16]. These properties indicate casein's potential as a carrier and encapsulating agent for nanofertilizers.

Moreover, copper nanoparticles (CuNPs) exhibit strong antimicrobial activity against both Gram-positive and Gram-negative bacteria, as well as against fungi, including plant pathogens [17, 18]. Phytopathogens pose a major threat to crop production and global food security by causing diseases that result in considerable agricultural and economic losses [19]. Notably, species of the genus *Fusarium* are among the most important groups of phytopathogenic fungi, affecting a wide variety of crops worldwide [20].

In our previous study, casein micelles (CuMC) were encapsulated within calcium carbonate microspheres to enhance their properties as carrier materials [21]. Building on this system, we further incorporated mycogenic CuNPs synthesized from *Fusarium graminearum* D and assessed the effects of the complex on maize growth and development, with the aim of employing it as a nanofertilizer. The novelty of this study lies in combining mycogenic CuNPs, CuMC, and $CaCO_3$ microspheres in a hierarchical composite and evaluating its physicochemical properties and effects on maize growth. To the best of our knowledge, this specific formulation has not previously been investigated as a nanofertilizer. The antimicrobial activity of CuNPs against bacterial and fungal plant pathogens was also evaluated. This approach offers the potential to prolong copper release from the nanofertilizer and to precisely control the dosage absorbed by plants, thereby improving agricultural efficiency while supporting environmental sustainability.

2. Materials and methods

2.1. Biosynthesis and characterization of physicochemical properties of CuNPs

2.1.1. Fungal extract preparation and mycosynthesis of CuNPs

Fungal extract from *Fusarium graminearum* D was used for the synthesis of CuNPs. The strain was cultured in Potato Dextrose Broth (PDB, A&A Biotechnology, Gdańsk, Poland) for 7 d at 25 °C in shaking conditions (140 revolutions per minute; rpm). Fungal biomass was subsequently centrifuged at 8000 rpm for 10 min (Sorvall Legend X1R, Thermo Scientific, Waltham, MA, USA), washed three times with sterile distilled water, and resuspended in sterile water (10 ml of water for 1 g of biomass) for 4 d for the purpose of fungal cell autolysis. Next, the autolysate was centrifuged (4500 rpm, 5 min), passed through sterile filter paper, and used for the synthesis of CuNPs.

F. graminearum D autolysate was challenged with 1 M aqueous solution of $CuSO_4 \cdot 5\ H_2O$ in a 4:1 ratio (v/v). The obtained mixture was combined with 30% ascorbic acid (AA) to a final concentration of 2% and then mixed on a magnetic stirrer (500 rpm, 70 °C) for 3 h. Finally, biosynthesized

CuNPs were centrifuged (10 000 rpm, 10 min, 4 °C), washed thrice using sterile distilled water in order to dispose of unwanted components, and the obtained pellet was frozen at −80 °C, lyophilized for 24 h (LyoQuest, Telstar, Terrassa, Spain), and converted into powder form with a mortar and pestle.

2.1.2. Detection and characterization of CuNPs

Confirmation of CuNPs synthesis was carried out by visual observation of the reaction mixture and UV–Vis spectroscopy (NanoDrop One, Thermo Fisher Scientific, Waltham, MA, USA) over the wavelength range of 200–800 nm with a resolution of 1 nm.

Transmission electron microscopy (TEM) and energy dispersive x-ray (EDX) spectroscopy were performed to determine the morphology and elemental composition of NPs using a FEI Tecnai 12 microscope (FEI Company, Hillsboro, OR, USA) at an acceleration voltage of 100 kV. Prior to the analysis, the CuNP aqueous solution was deposited onto a carbon-coated nickel grid (mesh size 400 μm) and dried overnight at room temperature.

The crystalline structure of CuNPs was evaluated by powder x-ray diffraction (XRD) analysis, which was performed using a Rigaku MiniFlex 600 diffractometer (Rigaku, Tokyo, Japan) with Ni filter and CuKα ($\lambda = 1.54059$ Å) radiation source. Diffraction was recorded within the 2θ range of 5–120°, and the obtained diffractograms were compared to the standard database of the International Centre for Diffraction Data.

Fourier-transform infrared (FTIR) spectroscopy was employed to identify functional groups of biomolecules associated with the nanoparticle surface. Powder CuNPs were combined with KBr (1:100, w/w), and then analyzed using Bruker ALPHA II spectrophotometer (Bruker Optics, Billerica, MA, USA) in the attenuated total reflection mode in the range of 4000–400 cm^{-1} at the resolution of 4 cm^{-1}.

The size distribution of CuNPs was determined by nanoparticle tracking analysis (NTA) performed using NanoSight LM20 (NanoSight Ltd, Malvern, United Kingdom). Measurement conditions used for the analysis include temperature: 22 °C, viscosity: 0.95 cP, frames per second: 30.00, measurement time: 178 s, and drift velocity: 0 nm s^{-1}. The obtained results were analyzed using software provided by the manufacturer (NanoSight version 2.3).

Zeta potential measurements were used to evaluate nanoparticle stability using a Zetasizer ZS90 (Malvern Panalytical, Malvern, United Kingdom). CuNPs were analyzed at 25 °C, with 120 s as the calibration time, and water as a dispersant (refractive index: 1.33, viscosity: 0.89 cP, dielectric constant: 78.5), at pH 7. Zetasizer software version 6.32 was used to analyze the obtained data.

2.2. Synthesis and characterization of casein-CuNPs complex (CuMC)

2.2.1. Preparation of CuMC complex

For the synthesis of CuMC complex, 1% of sodium caseinate in 0.01 N NaOH was mixed on a magnetic stirrer until a clear solution was obtained. Next, powdered CuNPs (50, 100, 150, and 300 mg per 100 ml) were added and mixed for 15 min on a magnetic stirrer at 500 rpm. The complex was precipitated using 0.1 N HCl, centrifuged (10 000 rpm, 10 min), and the resulting pellet was washed three times with sterile distilled water, frozen at −80 °C, and lyophilized overnight (LyoQuest, Telstar, Terrassa, Spain).

2.2.2. Characterization

The size, shape, and distribution of the complex were determined using a transmission electron microscope (FEI Tecnai 12, FEI Company, Hillsboro, OR, USA) at an acceleration voltage of 100 kV. Sample preparation was conducted as described above for CuNPs.

The elemental composition of the complex at different concentrations of added CuNPs was determined by scanning electron microscopy with EDX spectroscopy (SEM-EDX) (1430 VP, LEO Electron Microscopy Ltd, England) at an acceleration voltage of 28 kV and 1000-fold magnification.

Inductively coupled plasma mass spectrometry (ICP-MS) was performed in order to measure the concentration of copper in all variants of the casein-CuNPs complex, using an ICP-MS 7500 CX spectrometer with collision chamber (Agilent Technologies, Santa Clara, CA, USA). Prior to analysis, 25 mg samples were digested for 1 h in a water bath (90 °C) with 0.5 ml of concentrated nitric acid and 0.5 ml of hydrogen peroxide, and the latter was added repeatedly until no precipitate remained, after which the volume was made up to 10 ml with Milli-Q water.

The stability of CuMC was assessed by measuring its zeta potential using the previously described procedure for CuNPs.

2.3. Preparation of casein-CuNPs complex encapsulated in calcium carbonate microspheres (CuMS)

2.3.1. Synthesis

Casein-CuNPs complex (150 mg of CuNPs per 100 ml of reaction mixture) was encapsulated in calcium carbonate microspheres by using freshly-prepared, cold (4 °C) ingredients. This concentration of CuNPs was selected because it yielded the highest copper incorporation efficiency per unit added, as demonstrated by SEM-EDX and ICP-MS analyses. Although the use of 300 mg of CuNPs per 100 ml resulted in a slightly higher absolute copper content in CuMC, this increase was not proportional to the twofold increase in the CuNPs input. 100 ml of 10% $CaCl_2$ and 30 ml of 10% citric acid were mixed (solution 1), and 3 g of casein-CuNPs complex was combined with 200 ml of 10% $(NH_4)_2CO_3$ and mixed on an orbital shaker until clear (solution 2). Then, solution 2 was added to solution 1, mixed for 30 min on a magnetic stirrer, and centrifuged (10 000 rpm, 10 min). The obtained pellet was washed twice with sterile distilled water and once with absolute ethanol, frozen at −80 °C, and lyophilized for 24 h (LyoQuest, Telstar, Terrassa, Spain).

2.3.2. Characterization

The morphology of calcium carbonate microspheres was evaluated by high resolution SEM (Quanta 3D FEG, Thermo Fisher Scientific, Waltham, MA, USA), while their elemental composition was determined by ICP-MS analysis (ICP-MS 7500 CX, Agilent Technologies, Santa Clara, CA, USA). The sample for analysis was prepared as mentioned above.

The zeta potential of CuMS was determined under the same measurement conditions and procedure as those used for CuNPs and CuMC.

The low-temperature nitrogen adsorption isotherms were measured at 77.5 K using the Autosorp iQ gas adsorption apparatus (Quantachrome, Boynton Beach, FL, USA). Before each measurement, the carbon samples were desorbed in a vacuum (below 10^{-3} Pa) at 323 K for 12 h.

Water adsorption and desorption analyses were used to assess the hydrophilicity of the microspheres. The measurements were performed using a Nicolet IS-50 FTIR spectrometer (Thermo Fisher Scientific, Waltham, MA, USA) with a Praying Mantis™ DRIFT chamber (Specac Ltd, Kent, England). Typically, 32 scans at a resolution of 4 cm^{-1} were collected in the range 8000–600 cm^{-1}. H_2O adsorption was carried out in the gas phase by passing the Ar stream through a bubbling water scrubber at 25 °C.

2.4. Evaluation of antimicrobial activity of CuNPs

2.4.1. Tested microorganisms

The antimicrobial activity of biosynthesized CuNPs was assessed against phytopathogenic bacterial strains, namely *Agrobacterium tumefaciens* IOR 911, *Pectobacterium carotovorum* PCM 2056, *Pseudomonas syringae* IOR 2188, and *Xanthomonas campestris* IOR 512, as well as phytopathogenic fungal strains, namely *Fusarium culmorum, Fusarium culmorum* IOR 2333, *Fusarium culmorum* DSM 114 849, *Fusarium graminearum* D, *Fusarium oxysporum, Fusarium oxysporum* IOR 342, *Fusarium oxysporum* D, *Fusarium poae* A, *Fusarium solani* IOR 825, and *Fusarium tricinctum*.

2.4.2. Antibacterial activity

The antibacterial activity of biosynthesized CuNPs was evaluated in accordance with the Clinical Laboratory Standards Institute (CLSI) protocol [22]. Briefly, bacterial strains were cultured for 24 h in Tryptic Soy Broth (TSB, Becton Dickinson, Franklin Lakes, NJ, USA) at 25 °C in shaking conditions (120 rpm). Bacterial inocula were prepared in sterile distilled water at a density of 0.5 in McFarland scale (1.5×10^8 colony forming units per ml; cfu ml^{-1}).

Minimal inhibitory concentration (MIC) was determined using a 2-fold dilution method in TSB medium in sterile 96-well plates in the concentration range of 64–2048 $\mu g\ ml^{-1}$. In each well, the final sample volume was 150 μl, and the final bacterial concentration was 1.5×10^6 cfu ml^{-1}. Sterile medium was used as a negative control, while the inoculated medium served as a positive control. The MIC value was defined as the lowest concentration of CuNPs for which no bacterial growth was observed visually after 24 h of incubation at 25 °C.

To determine the minimum bactericidal concentration (MBC) of CuNPs, 100 μl aliquots from wells without visible bacterial growth were spread onto Tryptic Soy Agar (TSA, Becton Dickinson, Franklin Lakes, NJ, USA) and incubated for 24 h at 25 °C. The lowest concentration of NPs that inhibited the growth of $\geqslant$99.9% of bacteria was read as MBC. All antibacterial analyses were performed in triplicate.

2.4.3. Antifungal activity

To assess CuNPs' inhibition of spore germination, MIC and minimum fungicidal concentration (MFC) were determined according to CLSI [22] with some modifications. Fungal strains were grown on Potato

Dextrose Agar (PDA, Becton Dickinson, Franklin Lakes, NJ, USA) for 14 d at 25 °C. Afterward, fungal colonies were washed with 10 ml of sterile distilled water to prepare spore suspensions, which were then filtered through a sterile cotton wool filter to remove remaining mycelia. Fungal spore suspensions with a density of 1×10^6 spores per ml were prepared.

MIC assay was performed as described earlier for bacteria, although using PDB medium. Inoculated plates were incubated for 2 d at 25 °C, and MIC values were determined as the lowest concentrations of CuNPs for which no fungal growth was noted.

Finally, 100 μl aliquots from wells with no visible fungal growth were spread onto PDA medium and incubated for 7 d at 25 °C. The lowest concentration of CuNPs that prevented visible fungal growth was considered the MBC. The antifungal assays were performed in triplicate.

2.5. Effect of CuNPs and CuNPs-based nanocomposites on seedling growth and chlorophyll content of maize

2.5.1. Sterilization of maize grains and growth conditions

The surface of maize (*Zea mays*) grains purchased from Torseed S.A. (Toruń, Poland) was sterilized for 30 min in 30% H_2O_2 and 70% ethanol (1:1, v/v), and then washed 5 times with sterile distilled water. The grains were positioned on 1/2 Murashige and Skoog (MS, Duchefa Biochemie, Haarlem, The Netherlands) medium with agar (8 g l^{-1}) in sterile Petri plates and incubated for 3 d at 22 ± 2 °C for germination.

The germinated grains were transferred to pots filled with 225 g of sterile sand to a depth of about 7 cm, covered with sand, and watered with an appropriate solution. Control grains were watered with Hoagland's solution (composition in Table S1), while the remaining three variants were treated with modified Hoagland solutions, namely the Cu source was substituted by CuNPs, casein micelles complexed with CuNPs (CuMC), and casein-CuNPs complex encapsulated in calcium carbonate microspheres (CuMS). The final copper content in each solution was determined by ICP-MS and set to 0.012 ppm. The analyzed variants were cultured in 25 replicates. Plants were watered as needed throughout their growth. 30-day-old plantlets were harvested, and their length and fresh and dry weights were measured, while leaves were frozen in liquid nitrogen and stored at −80 °C for chlorophyll content analysis.

2.5.2. Estimation of growth parameters

The lengths of shoots and roots were measured with a ruler in centimeters. Fresh and dry weight was estimated in milligrams, separately for leaves, stems, and roots.

2.5.3. Chlorophyll content

The leaf chlorophyll content in maize was calculated following the method by Witham *et al* [23]. From each variant 0.1 g of leaf tissue was ground in liquid nitrogen, extracted using 1.5 ml of cold 80% acetone, and centrifuged at 5000 × g for 5 min (Eppendorf 5424 R, Eppendorf SE, Hamburg, Germany). The supernatant was collected into a 15 ml test tube, and the extraction was repeated 6 times until the green tint disappeared. Subsequently, the absorbance of the supernatant was measured at 645 and 663 nm using a NanoDrop One (Thermo Fisher Scientific, Waltham, MA, USA). Chlorophyll content was determined using four biological replicates per treatment, with each biological replicate measured in at least two technical replicates (table S2). For the quantification of chlorophyll, the following formulas were used:

$$\text{Total chlorophyll (mg per g of FW)} = [20.2 \times (A\lambda_{645\text{nm}}) + 8.02 \times (A\lambda_{663\text{nm}})] \times \frac{V}{1000 \times FW} \quad (1)$$

$$\text{Chlorophyll a (mg per g of FW)} = [12.7 \times (A\lambda_{663\text{nm}}) - 2.69 \times (A\lambda_{645\text{nm}})] \times \frac{V}{1000 \times FW} \quad (2)$$

$$\text{Chlorophyll b (mg per g of FW)} = [22.9 \times (A\lambda_{645\text{nm}}) - 4.68 \times (A\lambda_{663\text{nm}})] \times \frac{V}{1000 \times FW} \quad (3)$$

where FW means the fresh leaf weight (g) and V is the final volume of the extract (ml).

2.5.4. Copper content

The concentration of copper present in the dry leaves, stems, and roots was assessed using Thermo Scientific iCE3300 FL (Waltham, MA, USA) atomic absorption spectrometer. Samples of 500 mg were incinerated in 550 °C for 24 h, and then digested and prepared as described previously for ICP-MS. Copper content was determined using one to three biological replicates per treatment.

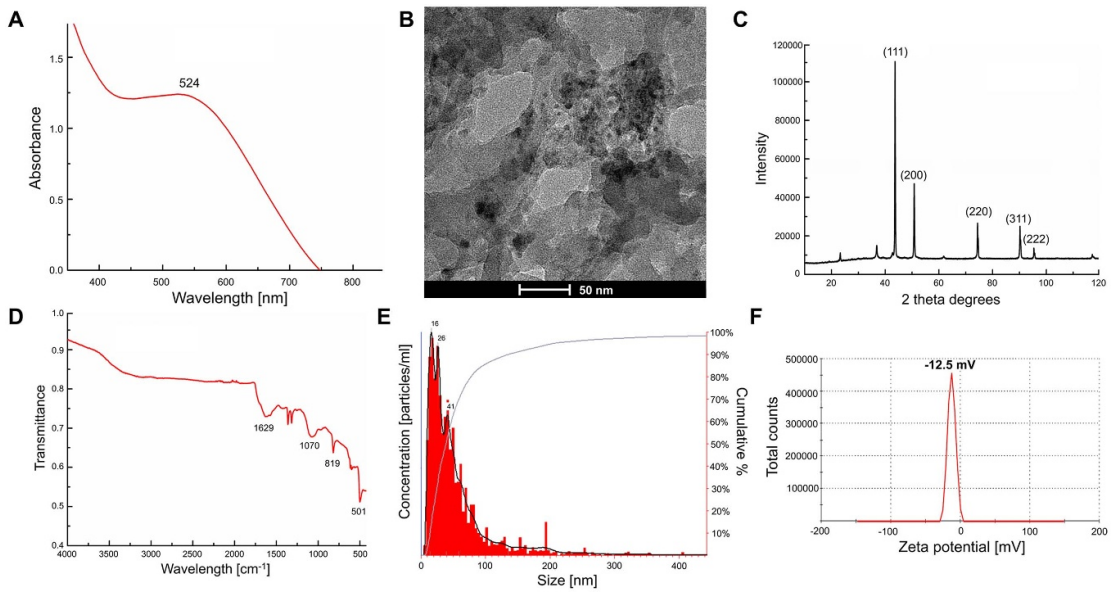

Figure 1. Detection and physicochemical characterization of CuNPs: (A) UV–Vis spectrum, (B) TEM micrograph, (C) x-ray diffractogram, (D) FTIR spectrum, (E) size distribution from NTA, (F) zeta potential.

2.6. Statistical analysis

Statistical analyses were performed using GraphPad InStat software version 3.06 (GraphPad Software, Boston, MA, USA). Data is presented as the mean ± standard deviation (SD). Normality was assessed using the Kolmogorov-Smirnov test, while homogeneity of variance was evaluated using Bartlett's test. Differences among the treatments were analyzed using one-way ANOVA, followed by the Tukey-Kramer multiple comparisons test. Differences were considered statistically significant at $p \leqslant 0.05$.

3. Results

3.1. Detection and characterization of mycosynthesized CuNPs

The formation of a red-brown precipitate in the reaction mixture indicated the synthesis of CuNPs, which was further confirmed by UV–Vis spectroscopy, which revealed a characteristic absorbance maximum at 524 nm (figure 1(A)). TEM micrographs showed the presence of spherical CuNPs with an average diameter of 8.43 nm (figure 1(B)). The elemental composition obtained from EDX analysis revealed 68.69% carbon, 17.49% copper, 6.8% oxygen, 5% chlorine, 1.45% sulfur, and 0.54% potassium (table S3).

The x-ray diffractogram (figure 1(C)) of CuNPs demonstrated peaks at 43.29°, 50.42°, 74.08°, 89.87°, and 95.08°, which correspond to (1 1 1), (2 0 0), (2 2 0), (3 1 1), and (2 2 2) crystallographic planes, respectively. XRD results confirmed the formation of CuNPs exhibiting a cubic phase structure, as indicated by JCPDS file no. 04–0836. The FTIR spectrum showed absorbance bands at 1629, 1070, 819, and 501 cm^{-1}, as presented in figure 1(D). NTA demonstrated that the average size of CuNPs was 69 nm (figure 1(E)), while Zeta potential measurement (figure 1(F)) revealed the synthesized nanoparticles to be negatively charged (−12.5 mV).

3.2. Characterization of casein-CuNPs complex

According to TEM analysis results, CuMC had an irregular shape and a mean diameter of 133.65 nm, with most being in the range of 73–98 nm (figure 2(A)). SEM-EDX (figures 2(B)–(D)) confirmed the presence of copper in the complex, which rose with the increase of CuNPs concentration in the mixture, and reached its peak in the sample with 150 mg of CuNPs, where copper constituted 23% of all elements. Other elements present in casein were also detected, including carbon, oxygen, nitrogen, phosphorus, and sulfur (table S4). ICP-MS data also showed that the highest binding effectiveness between CuNPs and casein, with the lowest amount of CuNPs required, occurred at the concentration of 150 mg of CuNPs per 100 ml of the reaction mixture (12.26%), as presented in figure 2(E) A similar trend was observed with SEM-EDX analysis of the samples.

CuMC exhibited a negative surface charge, with a zeta potential of −23.6 mV (figure S1).

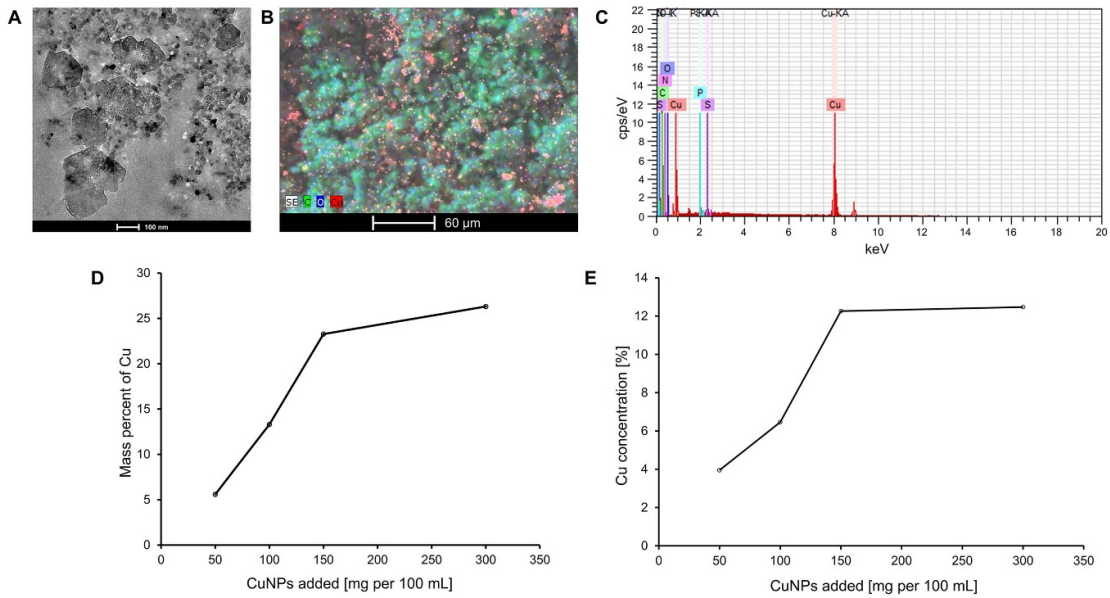

Figure 2. Physicochemical characterization of CuMC: (A) TEM micrograph, (B) elemental map from SEM-EDX at 150 mg of CuNPs per 100 ml, (C) elemental composition from SEM-EDX at 150 mg of CuNPs per 100 ml, (D) mass percent of copper from SEM-EDX at various concentrations of added CuNPs, (E) copper concentration in CuMC [%] measured by ICP-MS at various concentrations of added CuNPs.

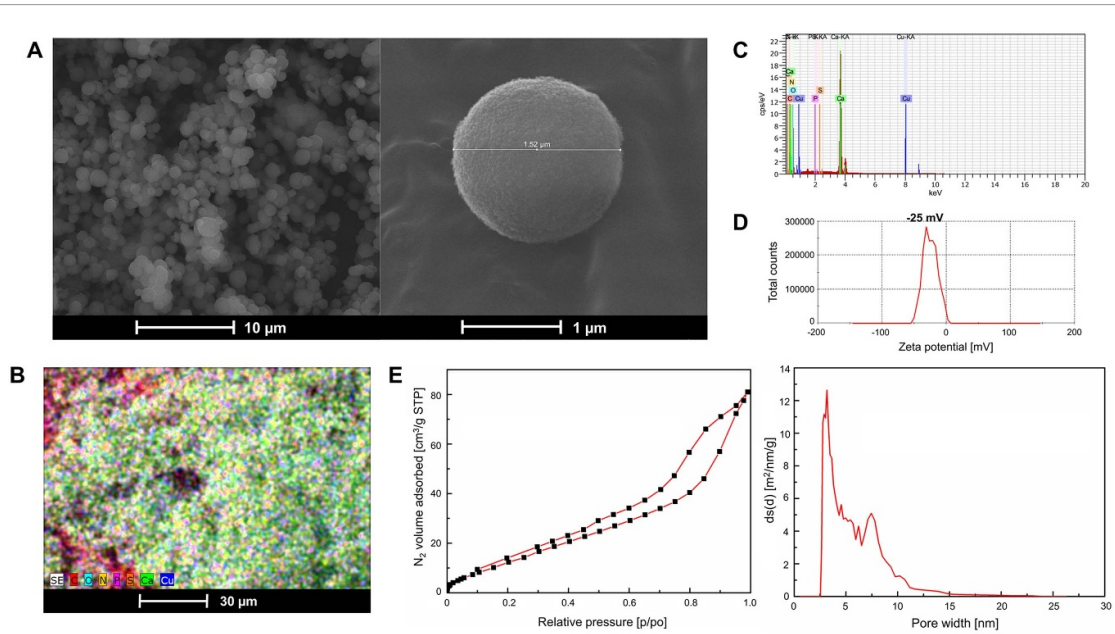

Figure 3. Physicochemical characterization of CuMS: (A) SEM micrographs, (B) elemental map from SEM-EDX, (C) elemental composition from SEM-EDX, (D) zeta potential, (E) N_2 adsorption and pore width analysis.

3.3. Characterization of casein-CuNPs complex encapsulated in calcium carbonate microspheres

SEM analysis revealed that the microspheres were spherical, with an average diameter of 1.09 μm and a dominant diameter range of 0.84–1.1 μm (figure 3(A)). SEM-EDX analysis confirmed the presence of copper, as well as calcium, oxygen, and carbon (table 1, figures 3(B) and (C)).

Copper accounted for 1.39% of the CuMS sample, as demonstrated by ICP-MS analysis.

CuMS were negatively charged, with zeta potential of −25.0 mV (figure 3(D)).

Nitrogen adsorption results are presented in figure 3(E). CuMS exhibited BET specific surface area of 65 $m^2\ g^{-1}$, with pore volume of 0.111 $cm^3\ g^{-1}$, and pore surface area of 37 $m^2\ g^{-1}$. The pore-size distribution from density functional theory analyses revealed a mesoporous structure. The smallest pores on the tested surfaces were found to be larger than 3.16 nm, while the largest were larger than 5.06 nm. The characteristics of infrared absorption bands related to water molecules adsorbed on the surface, such as

Table 1. Elemental composition of CuMS from SEM-EDX.

Element	Mass %	Atomic %
Calcium	74.81	55.80
Oxygen	11.87	22.18
Carbon	7.80	19.41
Copper	5.51	2.59

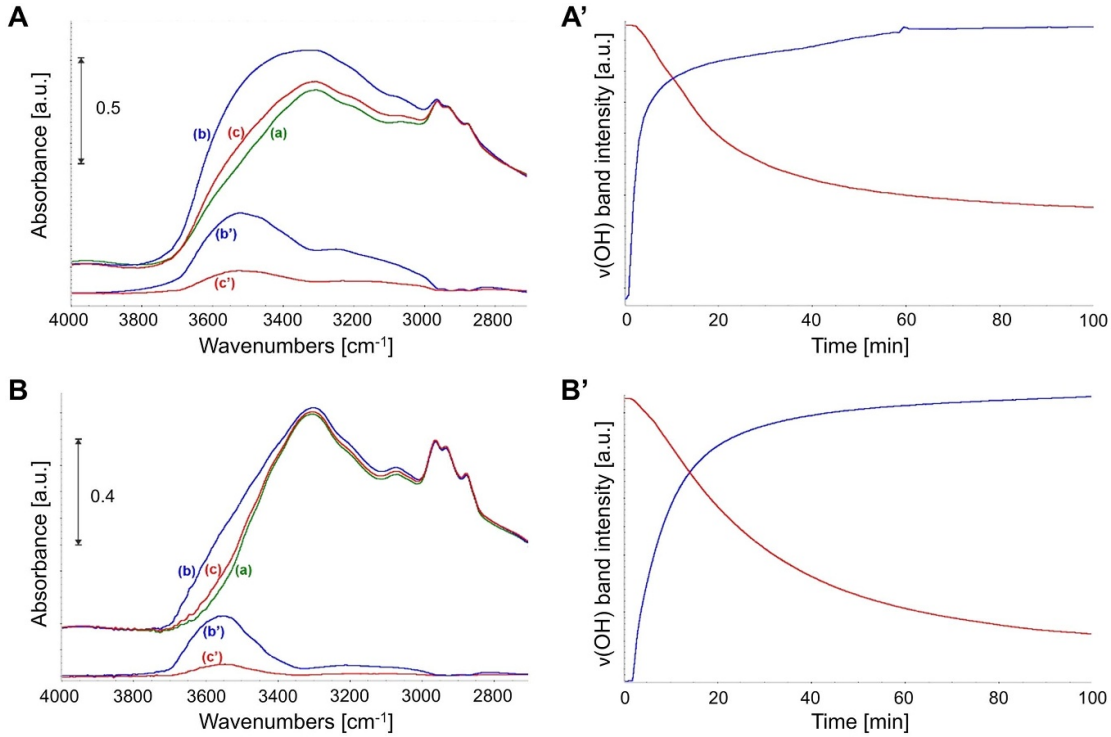

Figure 4. Spectroscopic investigation of H_2O adsorption on CuMS (A) and CuMC (B) at 25 °C. Left panel IR spectra of samples: (a) before H_2O adsorption, (b) after H_2O adsorption, (c) after H_2O desorption; (b') and (c') the differential spectra after H_2O adsorption and desorption, respectively. Right panel: time-dependent changes in the ν(OH) band intensities of CuMS and CuMC during the adsorption and desorption processes.

Table 2. Minimal inhibitory (MIC) and minimal bactericidal (MBC) concentration values [μg ml^{-1}] of CuNPs against bacterial phytopathogens.

Tested bacterial strains	MIC	MBC
Agrobacterium tumefaciens IOR 911	1024	2048
Pectobacterium carotovorum PCM 2056	>2048	>2048
Pseudomonas syringae IOR 2188	64	512
Xanthomonas campestris IOR 512	256	512

O–H stretching vibrations, are typically observed in the range of 3800 down to 2400 cm^{-1}. These broad bands correspond to hydrogen-bonded water molecules on the protein surface. Two distinct bands, perfectly visible in the differential spectra (b' and c') at 3550 and 3200 cm^{-1}, respectively, can be distinguished (figure 4), indicating that H_2O adsorption is faster than desorption for both tested samples. In addition, H_2O adsorption is faster for CuMS than for CuMC.

3.4. Evaluation of antimicrobial activity of CuNPs

3.4.1. Antibacterial activity

Antibacterial activity (MIC and MBC) of biosynthesized CuNPs against selected phytopathogens is shown in table 2. CuNPs exhibited the highest antibacterial activity against *P. syringae* (MIC = 64 μg ml^{-1} and MBC = 512 μg ml^{-1}), followed by *X. campestris* (MIC = 256 μg ml^{-1} and MBC = 512 μg ml^{-1}), and *A. tumefaciens* (MIC = 1024 μg ml^{-1} and MBC = 2048 μg ml^{-1}). MIC and MBC values were not determined for *P. carotovorum* in the tested concentration range.

Table 3. Minimal inhibitory (MIC) and minimal fungicidal (MFC) concentration values [μg ml^{-1}] of CuNPs against fungal phytopathogens.

Tested fungal strains	MIC	MFC
Fusarium culmorum	512	512
Fusarium culmorum IOR 2333	>2048	>2048
Fusarium culmorum DSM 114 849	512	512
Fusarium graminearum D	>2048	>2048
Fusarium oxysporum	>2048	>2048
Fusarium oxysporum IOR 342	1024	>2048
Fusarium oxysporum D	512	512
Fusarium poae A	2048	2048
Fusarium solani IOR 825	1024	>2048
Fusarium tricinctum	512	1024

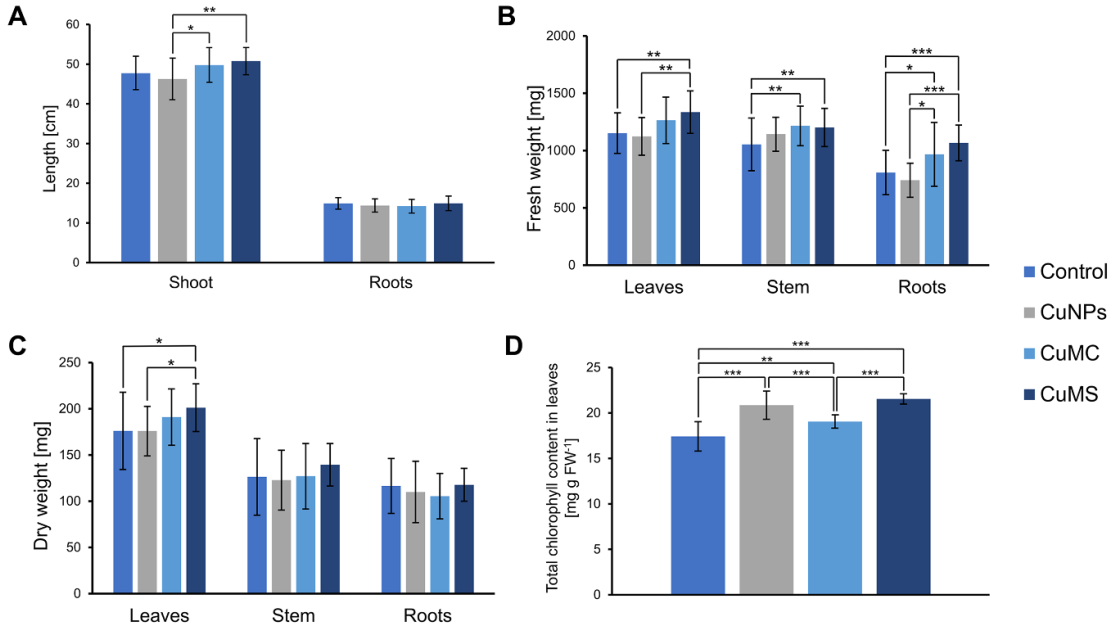

Figure 5. (A) Length, (B) fresh and (C) dry weight, and (D) total leaf chlorophyll content of 30 d-old maize plantlets after treatment with various sources of copper. Data presented as mean and standard deviation (SD), and statistical significance (p-value * $p \leqslant 0.05$, ** $p \leqslant 0.01$, *** $p \leqslant 0.001$).

3.4.2. Antifungal activity

The results of the antifungal activity analysis are presented in table 3. CuNPs showed equal inhibitory and fungicidal effect against *F. culmorum, F. culmorum* DSM 114 849, and *F. oxysporum* D (MIC and MBC = 512 μg ml^{-1}). *F. tricinctum* and *F. poae* A were less susceptible to CuNPs, with MIC values of 512 and 2048 μg ml^{-1}, and MFC values of 1024 and 2048 μg ml^{-1}, respectively. CuNPs inhibited spore germination of *F. oxysporum* IOR 342 and *F. solani* IOR 825 (MIC = 1024 μg ml^{-1}), but did not exhibit fungicidal activity against these strains.

3.5. Effect of CuNPs and CuNPs-based nanocomposites on seedling growth, and chlorophyll and copper content of maize

3.5.1. Estimation of growth parameters

The effects of maize treatment on the length, fresh, and dry weight were depicted in figure 5(A)–(C). CuMC treatment led to increased fresh weight of the stem and roots by 15.3% and 19.7%, respectively, whereas treatment with CuMS increased the fresh weight of leaves (16%), stem (14%), and roots (32.2%), as well as the dry weight of leaves (14.3%).

3.5.2. Leaf chlorophyll content

Treatment of maize with CuMS and CuNPs increased total leaf chlorophyll content (by 23.7 and 19.7%, respectively) compared to the control, while the application of CuMC resulted in a smaller increase (9.4%), as presented in figure 5(D). A similar trend was observed in chlorophyll a (17.6, 8.3, and 21.5%)

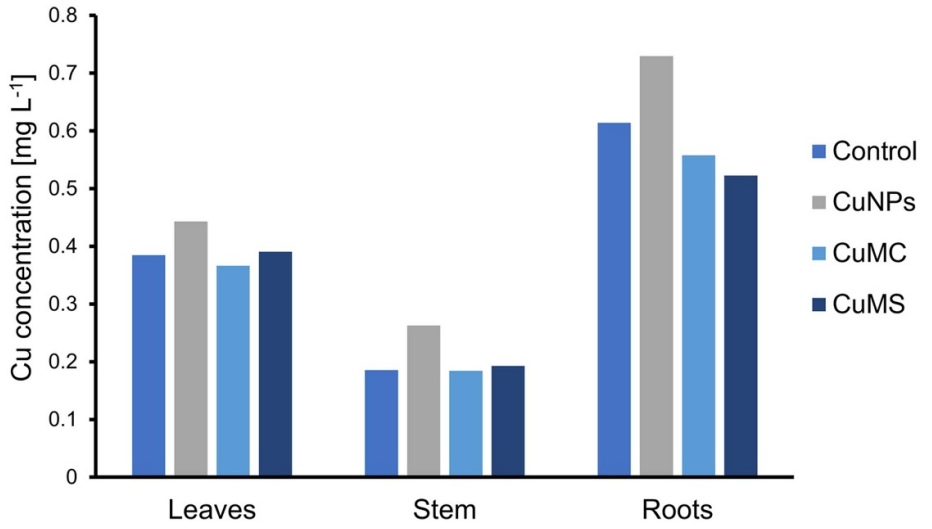

Figure 6. Copper concentration in dry leaves, stems, and roots of 30 d-old maize plantlets.

and chlorophyll b (20.8, 7.5, and 23.7%) content for CuNPs, CuMC, and CuMS treatment, respectively (figure S2).

3.5.3. Copper concentration in maize organs

Application of CuNPs caused a substantial increase in copper concentration in leaves, stems, and roots compared to the control, by 15.2, 41.7, and 18.8%, respectively (figure 6). Such a tendency was not observed after the application of CuMC and CuMS.

4. Discussion

4.1. Detection and characterization of mycosynthesized CuNPs

Bionanoparticles exhibit great potential for applications in numerous fields, such as medicine, agriculture, and environmental remediation [24]. Green nanotechnology, defined as the synthesis of nanomaterials from natural sources, has recently gained attention as an environmentally friendly approach [25, 26]. Among them, microbial synthesis is an effective method to synthesize CuNPs, which have been produced using bacteria, actinomycetes, and fungi [27–29]. In addition, AA, industrially produced by microorganisms, is used in nanoparticle synthesis as either main [30, 31] or additional reducing agent [32], while also preventing the oxidation of CuNPs and their agglomeration [30]. Utilization of renewable, naturally-derived, and non-toxic agents allows for sustainable synthesis process and minimizing the impact on the environment [33]. *Fusarium* spp. are one of the most popular fungi for nanoparticle synthesis, as they are easy to grow and process, and they exhibit bulk extracellular secretion, allowing for the production of green and sustainable nanoparticles [34]. To date, fungi from this genus, such as *Fusarium pseudonygamai, F. solani*, and *F. oxysporum*, have been used to synthesize a variety of nanoparticles, including silver, gold, copper, cobalt, and cadmium sulfide nanoparticles [35–37]. In the present work, CuNPs were synthesized by challenging *F. graminearum* D extract with copper sulfate and AA, resulting in the formation of a red-brown precipitate. In our study, the formation of CuNPs was confirmed by a UV–Vis absorption peak at 524 nm, which falls within the typical range of 520–600 nm [38, 39]. Furthermore, XRD results not only confirmed the crystalline structure of the CuNPs, but the recorded peaks were consistent with those reported by Gao *et al* [40], thereby confirming the structural integrity of mycogenic CuNPs. Evaluation of physicochemical properties of nanoparticles is of great importance since they influence their biological activity, consequently impacting their applications [41, 42]. Therefore, the obtained CuNPs were further characterized using TEM, NTA, FTIR and zeta potential measurements. Their size aligns with the results of other authors, such as Shende *et al* [43], who synthesized spherical CuNPs with a size in the range of 5–12 nm using a filtrate of *Aspergillus flavus*. However, the mean size of the CuNPs tested differed significantly in the TEM and NTA analysis (8.43 and 69 nm, respectively). The difference stems from the measurement techniques used in a dry environment and in a solution, where the hydrodynamic diameter is measured, which can include fungal-derived substances

and AA bound to the surface of the NPs. The role of fungal proteins and molecules in metal ions binding, reduction, nanoparticle formation and capping was demonstrated by several other authors [12, 44]. In our study it is also supported by the results of the EDX, which identified the presence of copper and other elements. Similar elements, namely carbon, oxygen, chlorine and potassium, were identified in CuNPs synthesized using *F. solani* extract, as reported by Khdir and Muhammed [45]. Furthermore, the presence of biomolecules on the surface of CuNPs was confirmed by FTIR analysis, which, based on the observed peaks, identified various functional groups, including carbonyl and hydroxyl groups. Similar findings were reported by Salas *et al* [32], who synthesized CuNPs using blueberry extract and, apart from a peak at 3137 cm^{-1}, identified peaks at 1612, 1050, and 584 cm^{-1} corresponding to C=O vibration, C=C bond, and the Cu fingerprint region, respectively. In a study on *Aspergillus kambarensis*-mediated synthesis of CuNPs, except the peaks at 3616, 2703, 2115, and 1410 cm^{-1}, the absorbance band at 819 cm^{-1} was found pointing to C=C bending, and can be assigned to alkenes [39]. The latter band was also found in the present study. In addition, Lu *et al* [46] obtained an FTIR spectrum of pure AA, with two peaks close to those observed in our results, namely at 1652 and 1045 cm^{-1}, corresponding to C=C stretching and –OH bending, respectively. Biomolecules from fungal metabolites, including proteins and polysaccharides, are involved in the process of nanoparticle synthesis and coat their surface, providing stability and preventing aggregation [42, 47]. The stability of nanoparticles is reflected by the zeta potential value, where the higher the absolute value (above 30 mV), the greater the stability of the nanoparticles [48, 49]. The obtained CuNPs, unlike those synthesized from *Aspergillus terreus* filtrate and copper acetate, showing the charge of −33.7 mV [50], were moderately stable (zeta potential value at −12.5 mV).

4.2. CuNPs-casein micelles (CuMC)

Casein micelles are considered natural carriers for bioactive compounds due to their porous structure, as well as very good biodegradability and biocompatibility [16, 51]. They have been used to encapsulate drugs and other substances, like paclitaxel and resveratrol, for protection against rapid degradation [52, 53]. Various proteins can bind copper, such as cuproenzymes which use it as a cofactor, as well as copper transporters, and metallothioneins involved in the storage of this element [54]. In this study, CuNPs were combined with sodium caseinate at alkaline pH and then encapsulated in CuMC after acidification. This is possible due to pH-dependent changes in micellar structure, since increasing the pH causes the micelles to loosen, while lowering it below the isoelectric point of casein (pH 4.6–4.8) results in their tightening [16]. The average diameter of micelles synthesized in the present study (133.65 nm) falls within the range of 50–500 nm obtained by Du *et al* [55]. The added value of CuMC is the presence of minerals contained in this polymer, which include carbon, oxygen, and sulfur, and contribute to their stability and impact their biological activity [56]. These findings were confirmed in our study via SEM-EDX. The structure of CuMC can be modified by other macromolecules, such as chitosan, and phosphoserine peptides, in order to enhance their stability, and improve their carrier abilities [57–59].

CuMC exhibited moderate stability (Zeta potential −23.6 mV), similarly to casein nanocapsules with curcumin described by Hooda *et al* [60] (−20.4 mV).

4.3. CuNPs-casein complex with calcium carbonate microspheres

Porous inorganic materials, with their high stability and durability, have attracted attention as carriers for sustained release of various substances [61]. Calcium carbonate is an abundant compound, naturally found in eggshells and the shells of marine organisms, and is often chosen as an encapsulating agent due to its good biocompatibility, slow degradation rate, and affordability [61, 62]. We encapsulated CuNPs-casein complex with calcium carbonate microspheres using the biomineralization method, similarly to Lee and colleagues [63] who immobilized carboxyl esterase in spherical calcium carbonate microspheres with a diameter range of 4–6 μm prepared using sodium carbonate and calcium chloride. Microspheres obtained in our study (average 1.09 μm), unlike those by Xiang *et al* [64] used as slow-release herbicide carriers, were almost two times smaller (2 μm). CuMS were moderately stable (zeta potential −25.0 mV), consistent with the negative surface potential of casein/$CaCO_3$ vaterite microspheres (−17 mV) [65]. Depending on synthesis conditions, microspheres can exhibit various pore sizes, which influence their potential applicability [66]. The nitrogen adsorption-desorption isotherm of the CuMS sample is characteristic of a type IV isotherm, indicating a predominantly mesoporous structure, just like calcium carbonate microspheres obtained by Bai *et al* [67]. The presence of a pronounced H3-type hysteresis loop suggests capillary condensation in mesopores with irregular shapes and possible pore constrictions. The corresponding pore-size distribution reveals a dominant population of small mesopores centered at approximately 3–4 nm, with additional contributions from wider mesopores up to

about 10 nm. A gradual tail extending toward larger pore widths indicates a heterogeneous and hierarchical pore network. Overall, the textural properties indicate a disordered mesoporous material with limited microporosity.

The presence of mesopores is particularly advantageous for water adsorption, as capillary condensation in this pore size range promotes effective moisture retention. In combination with the $CaCO_3$-based structure, mesoporosity and the inherently hydrophilic surface enhance the material's capacity to adsorb and retain water. This property may improve water availability in soil systems, especially under conditions of limited moisture. Consequently, such textural characteristics suggest a positive potential for agricultural applications, where enhanced water retention can support plant growth and soil conditioning.

The partial reversibility of the changes observed after the desorption process indicates the presence of both weakly and moderately strongly bound forms of water on the material surface. Analysis of the time-dependent evolution of the ν(OH) band intensity during H_2O adsorption and desorption reveals distinct differences in the rates of these processes, which points to high values of the Gibbs free energy of the adsorption process. At the same time, the absence of bands characteristic of strong hydrogen-bonded water molecules suggests, according to the literature, that the overall process is mainly governed by entropic factors [68]. Additionally, the observed differences in adsorption kinetics between CuMS and CuMC reflect the distinct surface and structural properties of the two materials.

4.4. Antimicrobial activity of CuNPs

Among metal nanoparticles, CuNPs are among the most promising antimicrobial agents, exhibiting activity against a wide range of microorganisms at relatively low production cost [69]. Although copper is commonly used as a fungicide, CuNPs, due to their unique properties, may be more effective than conventional copper-based antifungal agents in lower doses [17, 70]. CuNPs synthesized using an extract of *F. graminearum* exhibited antibacterial activity against three out of four tested strains, and antifungal activity against seven out of ten tested strains. CuONPs produced by a wet-chemistry approach also inhibited the growth of *A. tumefaciens* (MIC and MBC = 800 ppm), contrary to our results; they failed to inhibit the growth of *X. campestris* over the tested concentration range [71]. Additionally, CuONPs from *Ziziphus spina-christi* at 250 μg ml^{-1} inhibited the growth of *F. solani* by 91.17%, while CuNPs from *Stevia rebaudiana* leaf extract exhibited an activity against *F. oxysporum* (MIC = 75 μg ml^{-1}, MFC = 125 μg ml^{-1}), both showing better antifungal properties compared to our CuNPs [72, 73]. The toxicity mechanism of CuNPs is primarily mediated by the generation of reactive oxygen species, which damage cellular components, such as DNA, proteins, and lipids [74]. CuNPs also release Cu^{2+} ions, which bind to phosphate and sulfhydryl groups on the cell membrane, leading to depolarization, leakage of cellular contents, and metabolic collapse [69].

4.5. The effect of CuNPs, CuNPs-casein, CuNPs-casein complex with calcium carbonate microspheres on maize growth

One of the challenges the world is facing is the fast-growing human population and scarcity or resources, which necessitate more efficient agricultural practices in order to minimize hunger. However, prolonged use of conventional fertilizers in high doses has led to negative environmental consequences, such as water and air pollution, and deterioration of soil quality [6]. Moreover, the application of traditional fertilizers shows poor efficiency due to nutrient leaching, which causes economic losses [75]. Copper is a key micronutrient for plants, involved in various physiological processes, including photosynthesis, cellular respiration, enzymatic activity [76]. The appropriate level of this element is also critically important, as it becomes toxic at excessively high concentrations [77]. Therefore, the use of copper-based agrochemicals requires particular precision. In this study, CuNPs were combined with casein micelles and subsequently with calcium carbonate to form microspheres, to enable the resulting nanocomplexes to release nutrients in a controlled manner, thereby improving the efficiency of the nutrient delivery. This approach has the potential to enhance agricultural productivity, while promoting environmental sustainability. Studies have shown that application of nanofertilizers at optimized doses can improve plant growth without increasing copper accumulation in plant tissues compared with traditional forms of copper supplementation [78, 79]. Our results show that substitution of copper salt ($CuSO_4$) in Hoagland solution with CuMS, having the same copper content, increased fresh and dry weight of maize leaves. In addition, the stimulated fresh biomass of maize stems and roots was observed after both CuMC and CuMS treatments. The improvement in maize growth might be related to controlled copper release from CuMC and CuMS, driven by the gradual decomposition of casein and/or calcium carbonate. Maize root exudates are rich in various substances, including phenolic compounds, organic acids, carbohydrates, amino acids, and proteins, as well as enzymes [80]. As casein is built from α-helices and β-sheets, which are susceptible to proteolysis, it can be digested by enzymes secreted by

roots, while the organic acids may contribute to the surface dissolution of Ca^{2+} ions from the nanocomposite and then act as Ca^{2+} chelators [81–83]. In addition, as CuMC and CuMS composites showed high hydrophilic properties, the copper release from composites could be facilitated by water flow. Other authors reported improved maize growth after copper nanofertilizers application associated with gradual release of Cu, improved plant nutrient uptake, and pigment production [76, 84]. For instance, Lopez–Lima *et al* [76] reported more effective copper delivery to tomato plants after application of CuNPs in comparison to excessive uptake of Cu in plants treated with a commercial fungicide, while application of CuNPs-chitosan composite resulted in improved growth, yield, and chlorophyll content in maize [84]. This is consistent with our study's results, as chlorophyll levels increased after application of all tested composites. Other materials, such as hydroxyapatite, have been used to encapsulate fertilizers, with the authors correlating improved growth parameters with slower release of nutrients [85, 86]. However, the exact mechanisms behind CuMC and CuMS remain unclear and therefore require further evaluation.

5. Conclusions

In the present study, CuNPs synthesized from *F. graminearum* D were complexed with casein micelles and encapsulated within calcium carbonate microspheres in order to prolong nutrient release. CuNPs exhibited strong antimicrobial activity against phytopathogens. The obtained materials enhanced maize growth parameters and increased copper concentration and leaf chlorophyll content, highlighting their potential for dual agricultural use, both as fertilizers and as anti-phytopathogenic agents.

However, additional studies involving field evaluations, long-term environmental fate and ecotoxicological assessments, crop-specific performance, and large-scale production feasibility are necessary to validate its practical applicability in agricultural systems.

Acknowledgment

This research is part of the Project No. 2022/45/P/NZ9/01571 co-funded by the National Science Centre and the European Union Framework Programme for Research and Innovation Horizon 2020 under the Marie Skłodowska-Curie Grant Agreement No. 945339. For the purpose of Open Access, the author has applied a CC-BY public copyright license to any Author Accepted Manuscript (AAM) version arising from this submission.

Data availability statement

All data that support the findings of this study are included within the article (and any supplementary files).

Data openly available at: https://repod.icm.edu.pl/dataset.xhtml?persistentId=doi:10.18150/YIDOCN.

Supplementary data 5 available at: https://doi.org/10.1088/1361-6528/ae99eb/data1.

Author contributions

Julia Nadrowska 0009-0003-5538-4558
Formal analysis (equal), Investigation (equal), Methodology (equal), Writing – original draft (equal)

Joanna Trzcińska-Wencel 0000-0001-9119-0054
Formal analysis (equal), Investigation (equal), Methodology (equal), Resources (equal), Writing – original draft (equal)

Patrycja Golińska 0000-0001-9154-8191
Conceptualization (equal), Funding acquisition (equal), Investigation (supporting), Project administration (supporting), Resources (supporting), Supervision (equal), Writing – review & editing (supporting)

Marek Wiśniewski 0000-0003-3478-5371
Data curation (equal), Formal analysis (supporting), Validation (supporting), Writing – review & editing (supporting)

Sudhir Shende 0000-0002-2122-4543
Formal analysis (supporting), Methodology (supporting), Resources (supporting), Validation (supporting), Writing – review & editing (supporting)

Aniket Gade 0000-0002-1966-999X
Conceptualization (equal), Data curation (lead), Funding acquisition (equal), Resources (lead), Supervision (equal), Validation (lead), Writing – review & editing (lead)

References

[1] Shukla A K *et al* 2021 Deficiency of phyto-available sulphur, zinc, boron, iron, copper and manganese in soils of India *Sci. Rep.* **11** 19760
[2] Raliya R, Saharan V, Dimkpa C and Biswas P 2018 Nanofertilizer for precision and sustainable agriculture: current state and future perspectives *J. Agric. Food Chem.* **66** 6487–503
[3] Hänsch R and Mendel R R 2009 Physiological functions of mineral micronutrients (Cu, Zn, Mn, Fe, Ni, Mo, B, Cl) *Curr. Opin. Plant Biol.* **12** 259–66
[4] Jatav H S, Sharma L D, Sadhukhan R, Singh S K, Singh S and Rajput V D 2020 An overview of micronutrients: prospects and implication in crop production *Plant Micronutrients* (Springer) pp 1–30
[5] Choudhary S, Zehra A, Wani K I, Naeem M, Hakeem K R and Aftab T 2020 The role of micronutrients in growth and development: transport and signalling pathways from crosstalk perspective *Plant Micronutrients* (Springer) pp 73–81
[6] Zulfiqar F, Navarro M, Ashraf M, Akram N A and Munné-bosch S 2019 Nanofertilizer use for sustainable agriculture: advantages and limitations *Plant Sci.* **289** 110270
[7] Islam F, Shohag S, Uddin M D J, Islam M D R, Nafady M H, Akter A, Mitra S, Roy A, Emran T B and Cavalu S 2022 Exploring the journey of zinc oxide nanoparticles (ZnO-NPs) toward biomedical applications *Materials* **15** 2160
[8] Sheteiwy M S, Shaghaleh H, Hamoud Y A, Holford P, Shao H, Qi W, Hashmi M Z and Wu T 2021 Zinc oxide nanoparticles: potential effects on soil properties, crop production, food processing, and food quality *Environ. Sci. Pollut. Res.* **28** 36942–66
[9] Tran H-V, Ngo N M, Medhi R, Srinoi P, Liu T, Rittikulsittichai S and Lee T R 2022 Multifunctional iron oxide magnetic nanoparticles for biomedical applications: a review *Materials* **15** 503
[10] Hornak J 2021 Synthesis, properties, and selected technical applications of magnesium oxide nanoparticles: a review *Int. J. Mol. Sci.* **22** 12752
[11] Anjum S, Vyas A and Sofi T 2023 Fungi-mediated synthesis of nanoparticles: characterization process and agricultural applications *J. Sci. Food Agric.* **103** 4727–41
[12] Nassar A-R A, Atta H M, Abdel-rahman M A, El Naghy W S and Fouda A 2023 Myco-synthesized copper oxide nanoparticles using harnessing metabolites of endophytic fungal strain *Aspergillus terreus*: an insight into antibacterial, anti-*Candida*, biocompatibility, anticancer, and antioxidant activities *BMC Complement. Med. Ther.* **23** 261
[13] Sidhu A K, Agrawal S B, Verma N, Kaushal P and Sharma M 2025 Fungal-mediated synthesis of multimetallic nanoparticles: mechanisms, unique properties, and potential applications *Front. Nanotechnol.* **7** 1549713
[14] Elkalla E, Khizar S, Tarhini M, Lebaz N, Zine N, Jaffrezic-renault N, Errachid A and Elaissari A 2023 Core-shell micro/nanocapsules: from encapsulation to applications *J. Microencapsul.* **40** 125–56
[15] Głąb T K and Boratyński J 2017 Potential of casein as a carrier for biologically active agents *Top. Curr. Chem.* **375** 71
[16] Sadiq U, Gill H and Chandrapala J 2021 Casein micelles as an emerging delivery system for bioactive food components *Foods* **10** 1965
[17] Malandrakis A A, Kavroulakis N and Chrysikopoulos C V 2019 Use of copper, silver and zinc nanoparticles against foliar and soilborne plant pathogens *Sci. Total Environ.* **670** 292–9
[18] Nkosi N C, Basson A K, Ntombela Z G, Dlamini N G and Pullabhotla R V S R 2024 A review on bioflocculant-synthesized copper nanoparticles: characterization and application in wastewater treatment *Bioengineering* **11** 1007
[19] Saberi Riseh R and Gholizadeh Vazvani M 2024 Unveiling methods to stimulate plant resistance against pathogens *Front. Biosci.* **29** 188
[20] Summerell B A 2019 Resolving *fusarium*: current status of the genus *Annu. Rev. Phytopathol.* **57** 323–39
[21] Gade A, Nadrowska J, Trzcińska-Wencel J, Wiśniewski M, Raut RRai M and Golińska P 2025 Casein-assisted biomineralization of calcium carbonate microspheres for enhanced surface and adsorption properties *Front. Bioeng. Biotechnol.* **13** 1654712
[22] Cockerill F 2012 *Methods for Dilution Antimicrobial Susceptibility Tests for Bacteria that Grow Aerobically: Approved Standard* 9th edn (Clinical and Laboratory Standards Institute)
[23] Witham F H, Blaydes D F and Devlin R M 1971 *Experiments in Plant Physiology* (Van Nostrand)
[24] Verma S K, Kumar P, Mishra A, Khare R and Singh D 2024 Green nanotechnology: illuminating the effects of bio-based nanoparticles on plant physiology *Biotechnol. Sustain. Mater.* **1** 1
[25] Alqarni L S, Alghamdi M D, Alshahrani A A and Nassar A M 2022 Green nanotechnology: recent research on bioresource-based nanoparticle synthesis and applications *J. Chem.* **2022** 1–31
[26] Bhandari G *et al* 2023 A perspective review on green nanotechnology in agro-ecosystems: opportunities for sustainable agricultural practices & environmental remediation *Agriculture* **13** 668
[27] Hassan S E-D, Salem S S, Fouda A, Awad M A, El-gamal M S and Abdo A M 2018 New approach for antimicrobial activity and bio-control of various pathogens by biosynthesized copper nanoparticles using endophytic actinomycetes *J. Radiat. Res. Appl. Sci.* **11** 262–70
[28] Noor S, Hassan M A, Aslam M A, Muhammad S A, Quosain Naqvi T, Batool Alvi G, Nagaraj H, Bilal Hussain S and Rotello V M 2025 Fungal biosystems for the fabrication of copper nanoparticles: an effective approach for the treatment of bacterial biofilms *ACS Appl. Mater. Interfaces* **17** 42706–16
[29] Rani S, Kumar P, Dahiya P, Mehta A, Dang A S and Suneja P 2025 Optimization, characterization and antibacterial activity of copper nanoparticles biosynthesized using *Pantoea agglomerans* CPHN2 *Indian J. Microbiol.* **65** 1345–56
[30] Alam M, Tabassum M, Mostofa S, Kumar Bishwas R, Sarkar D and Akter Jahan S 2023 The effect of precursor concentration on the crystallinity synchronization of synthesized copper nanoparticles *J. Cryst. Growth* **621** 127386

[31] Soltau Missio Pinheiro L D, Sentena N Z, Sangoi G G, Vizzotto B S, de Oliveira Pinto E, Pavoski G, Romano Espinosa D C, Machado A K and Leonardo da Silva W 2023 Copper nanoparticles from acid ascorbic: biosynthesis, characterization, *in vitro* safety profile and antimicrobial activity *Mater. Chem. Phys.* **307** 128110
[32] Salas Z H, Martínez Ávila A F, Hernández Orozco M M, Elizalde Peña E A, Palma Tirado L, Baldenegro Pérez L A, Padilla Vaca F, Luna-bárcenas G and España Sánchez B L 2023 Green synthesis of copper nanoparticles and their formulation into face masks: an antibacterial study *Polym. Compos.* **44** 907–16
[33] Kumar A, Tyagi P K, Tyagi S and Ghorbanpour M 2024 Integrating green nanotechnology with sustainable development goals: a pathway to sustainable innovation *Discov. Sustain.* **5** 364
[34] Rai M, Bonde S, Golinska P, Trzcińska-Wencel J, Gade A, Abd-Elsalam K A, Shende S, Gaikwad S and Ingle A P 2021 *Fusarium* as a novel fungus for the synthesis of nanoparticles: mechanism and applications *J. Fungi* **7** 139
[35] Loa J D A, Hernández-jiménez M O, Rojas-Avelizapa L I, Rivas-castillo A M and Rojas-Avelizapa N G 2024 Characterization and participation of biomolecules in CdS-NPs synthesis from an aqueous extract of *Fusarium oxysporum* with potential application in metal detection *Biocatal. Agric. Biotechnol.* **58** 103131
[36] Soliman M K Y, Abu-elghait M, Salem S S and Azab M S 2024 Multifunctional properties of silver and gold nanoparticles synthesis by *Fusarium pseudonygamai Biomass Convers. Biorefin.* **14** 28253–70
[37] El-wahab G M M A, Khedr Y I, Masoud S A and Nassar A M K 2025 Carbendazim-chitosan and copper- and cobalt-fusarium nanoparticles biological activity against potato root rot disease caused by *Rhizoctonia solani Plant Nano Biol.* **11** 100136
[38] Natesan K, Ponmurugan P, Gnanamangai B M, Manigandan V, Joy S P J, Jayakumar C and Amsaveni G 2021 Biosynthesis of silica and copper nanoparticles from *Trichoderma, Streptomyces* and *Pseudomonas* spp. evaluated against collar canker and red root-rot disease of tea plants *Arch. Phytopathol. Plant Prot.* **54** 56–85
[39] Gholami-shabani M, Sotoodehnejadnematalahi F, Shams-ghahfarokhi M, Eslamifar A and Razzaghi-abyaneh M 2022 Physicochemical properties, anticancer and antimicrobial activities of metallic nanoparticles green synthesized by *Aspergillus kambarensis IET Nanobiotechnol.* **16** 1–13
[40] Gao S, Jia X, Yang J and Wei X 2012 Hierarchically micro/nanostructured porous metallic copper: convenient growth and superhydrophilic and catalytic performance *J. Mater. Chem.* **22** 21733
[41] Naveen K V, Sathiyaseelan A, Mariadoss A V A, Xiaowen H, Saravanakumar K and Wang M-H 2021 Fabrication of mycogenic silver nanoparticles using endophytic fungal extract and their characterization, antibacterial and cytotoxic activities *Inorg. Chem. Commun.* **128** 108575
[42] Oyebamiji A K, Akintelu S A, Afolabi S O, Ebenezer O, Akintayo E T and Akintayo C O 2025 A comprehensive review on mycosynthesis of nanoparticles, characteristics, applications, and limitations *Plasmonics* **20** 6919–37
[43] Shende S, Bhagat R, Raut R, Rai M and Gade A 2021 Myco-fabrication of copper nanoparticles and its effect on crop pathogenic fungi *IEEE Trans. Nanobiosci.* **20** 146–53
[44] Liu F, Shah D S and Gadd G M 2021 Role of protein in fungal biomineralization of copper carbonate nanoparticles *Curr. Biol.* **31** 358–368.e3
[45] Khdir K A and Muhammed S M 2026 Eco-friendly nanoparticles from *Fusarium solani* suppress biofilms and quorum sensing in *Pseudomonas aeruginosa Nanoscale Adv.* **8** 80–96
[46] Lu R, Hao W, Kong L, Zhao K, Bai H and Liu Z 2023 A simple method for the synthesis of copper nanoparticles from metastable intermediates *RSC Adv.* **13** 14361–9
[47] Zhou Y, Nguyen H N, Peña-bahamonde J, Robles-hernandez F C, Gimenes L J and Rodrigues D F 2024 The role of secondary metabolites in the production of CuO nanoparticles by fungi: a physiological and metabolic approach *Environ. Sci.: Nano* **11** 4487–500
[48] Guilger-casagrande M, Germano-costa T, Bilesky-josé N, Pasquoto-stigliani T, Carvalho L, Fraceto L F and de Lima R 2021 Influence of the capping of biogenic silver nanoparticles on their toxicity and mechanism of action towards *Sclerotinia sclerotiorum J. Nanobiotechnol.* **19** 53
[49] Restrepo C V and Villa C C 2021 Synthesis of silver nanoparticles, influence of capping agents, and dependence on size and shape: a review *Environ. Nanotechnol. Monit. Manage.* **15** 100428
[50] El-naggar M E, Hasanin M and Hashem A H 2022 Eco-friendly synthesis of superhydrophobic antimicrobial film based on cellulose acetate/polycaprolactone loaded with the green biosynthesized copper nanoparticles for food packaging application *J. Polym. Environ.* **30** 1820–32
[51] Wang X and Zhao Z 2022 Improved encapsulation capacity of casein micelles with modified structure *J. Food Eng.* **333** 111138
[52] Cuggino J C, Picchio M L, Gugliotta A, Bürgi M, Ronco L I, Calderón M, Etcheverrigaray M, Alvarez Igarzabal C I, Minari R J and Gugliotta L M 2021 Crosslinked casein micelles bound paclitaxel as enzyme activated intracellular drug delivery systems for cancer therapy *Eur. Polym. J.* **145** 110237
[53] Khan M A, Cheng K-W and Hemar Y 2025 Fabrication of re-assembled casein micelles for improved stability and protection of resveratrol through encapsulation *Lwt* **218** 117508
[54] Collins J F 2021 Copper nutrition and biochemistry and human (patho)physiology *Advances in Food and Nutrition Research* ed M Eskin (Academic) pp 311–64
[55] Du Z, Xu N, Yang Y, Li G, Tai Z, Li N and Sun Y 2023 Study on internal structure of casein micelles in reconstituted skim milk powder *Int. J. Biol. Macromol.* **224** 437–52
[56] Erukainure O L, Salau V F, Alabi O O, Ebuehi O A T, Koorbanally N A and Islam M S 2020 Casein micelles from bovine milk exerts neuroprotection by stalling metabolic complications linked to oxidative brain injury *Metab. Brain Dis.* **35** 1417–28
[57] Ramezani H, Sazegar H and Rouhi L 2024 Chitosan-casein as novel drug delivery system for transferring *Phyllanthus emblica* to inhibit *Pseudomonas aeruginosa BMC Biotechnol.* **24** 101
[58] Wang Q, Liu Y, Ma Y, Lu Y, Huang L and Wang Z 2025 The composition, microstructure, interaction with polysaccharides of casein micelles and their potential application as drug delivery-a review *Food Biosci.* **65** 106068
[59] Zhou L *et al* 2025 Micellar casein were constructed to improve the encapsulation efficiency of algae oil docosahexaenoic acid by transglutaminase-coupled phosphoserine peptide chelating with Ca^{2+} *Int. J. Biol. Macromol.* **297** 139939
[60] Hooda A, Mann B, Sharma R, Tripathi A D, Rai H K, Singh S and Khosravi-darani K 2025 Designing of nanocapsules of curcumin using native casein micelles and their physicochemical, structural, stability and bioavailability analysis *J. Iran. Chem. Soc.* **22** 819–35
[61] Qiu N *et al* 2012 Calcium carbonate microspheres as carriers for the anticancer drug camptothecin *Mater. Sci. Eng. C* **32** 2634–40
[62] Al Omari M M H, Rashid I S, Qinna N A, Jaber A M and Badwan A A 2016 *Calcium Carbonate. Profiles of Drug Substances, Excipients and Related Methodology* (Academic) pp 31–132

[63] Lee C H, Jin E S, Lee J H and Hwang E T 2020 Immobilization and stabilization of enzyme in biomineralized calcium carbonate microspheres *Front. Bioeng. Biotechnol.* **8** 553591
[64] Xiang Y, Han J, Zhang G, Zhan F, Cai D and Wu Z 2018 Efficient synthesis of starch-regulated porous calcium carbonate microspheres as a carrier for slow-release herbicide *ACS Sustain. Chem. Eng.* **6** 3649–58
[65] Li Y, Li X, Cao Z, Xu Y, Gong Y and Shi X 2017 Fabrication of uniform casein/$CaCO_3$ vaterite microspheres and investigation of its formation mechanism *Cryst. Growth Des.* **17** 6178–88
[66] Cai Y, Chen Y, Hong X, Liu Z and Yuan W 2013 Porous microsphere and its applications *Int. J. Nanomed.* **8** 1111
[67] Bai W, Chen H, Li J, Cai W, Kong Y and Zuo X 2025 Calcium carbonate hollow microspheres encapsulated cellulose nanofiber/-sodium alginate hydrogels as a sequential delivery system *Int. J. Biol. Macromol.* **309** 142839
[68] Horiuchi S *et al* 2025 Low-entropy supramolecular crystals elucidating the inhomogeneity of interfacial water molecules at atomic resolution *Nat. Commun.* **16** 7588
[69] Pellosi D S *et al* 2025 Harnessing copper nanoparticles for antimicrobial applications: advances and challenges *Antibiotics* **14** 1170
[70] Tamm L *et al* 2022 Use of copper-based fungicides in organic agriculture in twelve european countries *Agronomy* **12** 673
[71] Varympopi A *et al* 2020 Bactericides based on copper nanoparticles restrain growth of important plant pathogens *Pathogens* **9** 1024
[72] Abdelhai M F, Shabaan R H, Kamal N M, Elemary E A, Abd-elhalim B T and Hassan E A 2024 Copper nanoparticles biosynthesis by *Stevia rebaudiana* extract: biocompatibility and antimicrobial application *AMB Express* **14** 59
[73] El-abeid S E, Mosa M A, El-tabakh M A M, Saleh A M, El-khateeb M A and Haridy M S A 2024 Antifungal activity of copper oxide nanoparticles derived from *Zizyphus spina* leaf extract against *Fusarium* root rot disease in tomato plants *J. Nanobiotechnol.* **22** 28
[74] Ramos-zúñiga J, Bruna N and Pérez-donoso J M 2023 Toxicity mechanisms of copper nanoparticles and copper surfaces on bacterial cells and viruses *Int. J. Mol. Sci.* **24** 10503
[75] Yadav A, Yadav K and Abd-elsalam K 2023 Nanofertilizers: types, delivery and advantages in agricultural sustainability *Agrochemicals* **2** 296–336
[76] Lopez-Lima D, Mtz-enriquez A I, Carrión G, Basurto-cereceda S and Pariona N 2021 The bifunctional role of copper nanoparticles in tomato: effective treatment for *Fusarium* wilt and plant growth promoter *Sci. Hortic.* **277** 109810
[77] Adrees M, Ali S, Rizwan M, Ibrahim M, Abbas F, Farid M, Zia-ur-rehman M, Irshad M K and Bharwana S A 2015 The effect of excess copper on growth and physiology of important food crops: a review *Environ. Sci. Pollut. Res.* **22** 8148–62
[78] Francis D V, Sood N and Gokhale T 2022 Biogenic CuO and ZnO nanoparticles as nanofertilizers for sustainable growth of *amaranthus hybridus Plants* **11** 2776
[79] Marmiroli M *et al* 2021 Copper oxide nanomaterial fate in plant tissue: nanoscale impacts on reproductive tissues *Environ. Sci. Technol.* **55** 10769–83
[80] Santangeli M, Steininger-mairinger T, Vetterlein D, Hann S and Oburger E 2024 Maize (*Zea mays* L.) root exudation profiles change in quality and quantity during plant development—a field study *Plant Sci.* **338** 111896
[81] Gaume A, Mächler F, De León C, Narro L and Frossard E 2001 Low-P tolerance by maize (*Zea mays* L.) genotypes: significance of root growth, and organic acids and acid phosphatase root exudation *Plant Soil* **228** 253–64
[82] Ma W, Tang S, Dengzeng Z, Zhang D, Zhang T and Ma X 2022 Root exudates contribute to belowground ecosystem hotspots: a review *Front. Microbiol.* **13** 937940
[83] Bělonožníková K, Černý M, Hýsková V, Synková H, Valcke RHodek O, Křížek T, Kavan D, Vaňková R, Dobrev P and Haisel D 2023 Casein as protein and hydrolysate: biostimulant or nitrogen source for *Nicotiana tabacum* plants grown *in vitro*? *Physiol. Plant.* **175** e13973
[84] Munir Y, Gul S, Iqbal Khan M and Bahadar Khan S 2024 Ecofriendly synthesis of copper oxide-chitosan nanocomposites and their efficacy as nano-pesticide and nano-fertilizer *Inorg. Chem. Commun.* **168** 112769
[85] Liu R and Lal R 2014 Synthetic apatite nanoparticles as a phosphorus fertilizer for soybean (*Glycine max*) *Sci. Rep.* **4** 5686
[86] Kottegoda N, Sandaruwan C, Priyadarshana G, Siriwardhana A, Rathnayake U A, Berugoda Arachchige D M, Kumarasinghe A R, Dahanayake D, Karunaratne V and Amaratunga G A J 2017 Urea-hydroxyapatite nanohybrids for slow release of nitrogen *ACS Nano* **11** 1214–21